J. Fluid Mech. (1986), *vol.* 169, *pp.* 275–292
Printed in Great Britain

Waves caused by a moving disturbance in a shallow channel of finite width

By R. C. ERTEKIN†, W. C. WEBSTER AND J. V. WEHAUSEN
Department of Naval Architecture & Offshore Engineering, University of California, Berkeley

(Received 11 July 1985 and in revised form 16 December 1985)

The flow created by an impulsively started pressure distribution travelling at a constant velocity in a shallow channel is investigated. The restricted Green–Naghdi theory of fluid sheets is used to perform the three-dimensional calculations. The results show remarkable similarity to model tests. In particular, these calculations predict the periodic generation of two-dimensional solitons in front of and travelling faster than the disturbance if the disturbance is large enough. Behind the disturbance a complicated, doubly corrugated set of waves is formed. The computations also predict that periodic creation of solitons is accompanied by a correspondingly periodic oscillation of the wave drag, as well as a dramatic increase in the mean wave drag.

1. Introduction

Let a body, typically a ship model, situated in a long water-filled basin of rectangular cross-section be set into motion, starting from rest, and maintain eventually a constant velocity parallel to the length of the basin. If the motion is not too far supercritical, it has been observed that two-dimensional waves spanning the tank are generated periodically and precede the model down the tank at supercritical speed. Hereafter we shall call these waves solitons.

The first mention of this phenomenon of which we are aware is in a report by Thews & Landweber (1935); the first published systematic experimental study seems to be by Graff (1962), although this was preceded by an earlier report by Sturtzel & Graff (1958). The phenomenon was rediscovered experimentally in the ship-model tank of the University of California, Berkeley in 1978 and more or less simultaneously in various other towing tanks. A systematic experimental investigation was begun in 1981, some results of which have already been reported (e.g. Huang *et al.* 1982*a*, *b*; Ertekin 1984; Ertekin, Webster & Wehausen 1984).

In 1982 Wu & Wu reported on some two-dimensional calculations in which quite clearly the same phenomenon was occurring, this time numerically. For these calculations Wu & Wu used shallow-water equations of Boussinesq-type derived earlier by Wu (1981). Some of these calculations are also reported in Huang *et al.* (1982*b*). In addition to these papers there are also papers reporting calculations using the Korteweg–de Vries equation or similar equations: Akylas (1984); Cole (1985); Mei (1986).

In connection with the experimental investigations at U. C., Berkeley numerical calculations were also undertaken, two-dimensional as in those of Wu & Wu, but using

† Present address: Department of Ocean Engineering, University of Hawaii, Honolulu.

some equations of Green & Naghdi (1976*b*) as well as those of Wu. The results are reported in Ertekin (1984) and a sample of them is given in Ertekin *et al.* (1984).

The calculations reported by Wu & Wu (1982) and by Ertekin *et al.* (1984) were for disturbances caused by a moving two-dimensional pressure distribution on the surface or by a moving bump on the bottom. Although the experimentally observed phenomenon of escaping solitons was confirmed by these calculations, they were not able by their very nature to exhibit one of the striking features of the towing-tank experiments, namely the generation of two-dimensional solitons by a moving three-dimensional disturbance. These solitons precede the disturbance, with the usual complicated three-dimensional wave motion following it. It is the purpose of this paper to present such calculations.

2. Green–Naghdi restricted theory

The equations that will be used for the calculations are those derived by Green & Naghdi (1976*b*) (hereafter the G–N equations) using the theory of Cosserat surfaces. Although these equations are discussed in Ertekin *et al.* (1984), some further remarks may be useful. As is noted in that paper, the only assumption besides that of an ideal fluid is that the vertical velocity component w is linear in z, the vertical coordinate, and that the horizontal components u and v are independent of z. Otherwise all conservation laws and invariance requirements are satisfied as well as the exact boundary conditions on the free surface and the bottom.

There is no formal limitation in the range of Froude number $\mathbb{F} = U/(gh_0)^{\frac{1}{2}}$ for which the model is applicable as long as $\mathbb{F} > 0$. Here U is the velocity of the disturbance, h_0 the mean water depth and g the acceleration of gravity. On the other hand, the nature of the initial assumption about the dependence of the velocity upon z would certainly leave one rather doubtful about its applicability in cases where $\mathbb{F}$ is quite small or where the physical situation is such that the assumption is clearly not satisfied even approximately. Nevertheless, since the equations satisfy exactly the depth-integrated conservation laws and the invariance requirements, one anticipates that they will never predict behaviour contradicting these laws. Hence, one does not expect solutions with free surfaces passing through the bottom or other physically unacceptable behaviour. They are, of course, limited by the assumption of an ideal fluid (an assumption not inherent in the method itself). On the other hand, there is no reason to suppose that the G–N equations will predict accurately, or even at all, an upper bound for soliton speed or a possible shape with a corner at the crest, both known results for 'exact' solutions of Euler's equations.

Since acceptability of the G–N equations seems doubtful for small values of $\mathbb{F}$, it seems appropriate to ask how small is 'small'. We have observed experimentally ship-generated solitons for values of $\mathbb{F}$ as low as 0.2, and in two dimensions have found them by numerical computation for $\mathbb{F} = 0.4$. That we didn't go lower was a consequence of computer limitation. Unfortunately, we are not able to show a direct comparison between computation and experimental measurement.

The G–N equations in the form used here are those for a 'single constrained director' and are not adequate to determine the local pressure within the fluid even though they do determine the depth-averaged pressure and the pressure on the bottom, and even though their solutions satisfy exactly the imposed pressure distribution on the free surface. However, within the framework of Cosserat surfaces, there are theories with more directors which can describe more complex flows, and still satisfy all conservation laws and invariance requirements (see, e.g. Green & Naghdi 1976*a*).

3. Equations of motion

It will be assumed that the fluid is inviscid and of constant density. It is not assumed that the motion is irrotational, and indeed it is not. This is one of the differences between the G–N equations and the equations used by Wu & Wu, a difference that makes the G–N equations more difficult to solve in three dimensions because there is no velocity potential.

We use a right-handed coordinate system with Oz directed upward, Ox to the right and Oy into the paper. The undisturbed free surface lies in the (x, y)-plane. The bottom is described by $z = -h(x, y, t)$. Eventually we shall take $h = \text{const.}$ and have channel walls at $y = \pm b$. The velocity components of a particle in the directions Ox, Oy, Oz, respectively, are given by u, v, w. As has already been stated above, the basic assumption underlying the G–N equations is that u and v do not depend upon z and that w is linear in z. Hence, we have $u = u(x, y, t)$, $v = v(x, y, t)$ and

$$w = w_0(x, y, t) + w_1(x, y, t)\, z.$$

The free surface will be described by $z = \eta(x, y, t)$, the pressure on the free surface by $\hat{p}(x, y, t)$ and the pressure on the bottom by $\bar{p}(x, y, t)$.

We may now write the G–N equations. Let

$$\mathrm{D} = \frac{\partial}{\partial t} + \boldsymbol{V}\cdot\boldsymbol{\nabla}, \quad \boldsymbol{\nabla} = \left(\frac{\partial}{\partial x}, \frac{\partial}{\partial y}\right), \quad \boldsymbol{V} = (u, v). \tag{1}$$

Then conservation of mass becomes

$$\eta_t + \boldsymbol{\nabla}\cdot\{(\eta + h)\, \boldsymbol{V}\} = -h_t, \tag{2}$$

and conservation of momentum

$$\mathrm{D}\boldsymbol{V} + g\boldsymbol{\nabla}\eta + \frac{\boldsymbol{\nabla}\hat{p}}{\rho} = -\tfrac{1}{6}\{-\mathrm{D}^2 h\boldsymbol{\nabla}[2\eta - h] + \mathrm{D}^2\eta\boldsymbol{\nabla}[4\eta + h] + (\eta + h)\,\boldsymbol{\nabla}[2\mathrm{D}^2\eta - \mathrm{D}^2 h]\}. \tag{3}$$

The vertical velocity w can be found explicitly once one has found u, v and η:

$$w = -\mathrm{D}h + \frac{(z + h)}{(\eta + h)}\mathrm{D}(\eta + h). \tag{4}$$

The pressure on the bottom is given by

$$\bar{p} = \rho g(\eta + h) + \tfrac{1}{2}\rho(\eta + h)(\mathrm{D}^2\eta - \mathrm{D}^2 h) + \hat{p}, \tag{5}$$

and the depth-integrated pressure, $\tilde{p} = \int p\, \mathrm{d}z$, by

$$\tilde{p} = \tfrac{1}{2}\rho g(\eta + h)^2 + \tfrac{1}{6}\rho(\eta + h)^2(2\mathrm{D}^2\eta - \mathrm{D}^2 h) + \hat{p}(\eta + h). \tag{6}$$

In the numerical calculations that will be shown later, h will be taken constant $= h_0$. The equations then simplify in an obvious way and become the following:

$$\eta_t + \boldsymbol{\nabla}\cdot\{(\eta + h_0)\, \boldsymbol{V}\} = 0, \tag{7}$$

$$\mathrm{D}\boldsymbol{V} + g\boldsymbol{\nabla}\eta + \frac{\boldsymbol{\nabla}\hat{p}}{\rho} = -\tfrac{1}{3}\{2\mathrm{D}^2\eta\, \boldsymbol{\nabla}\eta + (\eta + h_0)\, \boldsymbol{\nabla}\mathrm{D}^2\eta\}, \tag{8}$$

$$w = \frac{\mathrm{D}\eta(z + h_0)}{\eta + h_0}, \tag{9}$$

$$\bar{p} = \rho g(\eta + h_0) + \tfrac{1}{2}\rho(\eta + h_0)\, \mathrm{D}^2\eta + \hat{p}, \tag{10}$$

$$\tilde{p} = \tfrac{1}{2}\rho g(\eta + h_0)^2 + \tfrac{1}{3}\rho(\eta + h_0)^2\, \mathrm{D}^2\eta + \hat{p}(\eta + h_0). \tag{11}$$

We recall that the solutions to these equations satisfy the exact boundary conditions on the free surface, i.e. $p = \hat{p}$, $\mathrm{D}\eta - w = 0$, and at the bottom, i.e. $\mathrm{D}h + w = 0$, as well as all conservation laws and invariance requirements. We recall also that the theory does not provide p within the fluid. We add the boundary conditions

$$v(x, \pm b, t) = 0 \tag{12}$$

on the channel walls. For initial conditions we take

$$(u, v) = 0, \quad \eta = \frac{-\hat{p}}{\rho g}. \tag{13}$$

4. The three-dimensional disturbance

In order to model with the least effort the effect of a ship moving down a channel, we shall take $\hat{p}$ in the form $\hat{p}(x+Ut, y)$, where $\hat{p} = 0$ outside a rectangle symmetric about the x- and y-axes with length L and breadth B. Within the quarter of the rectangle, $0 < x < \frac{1}{2}L$, $0 < y < \frac{1}{2}B$, $\hat{p}$ is defined as

$$\hat{p}(x, y) = A f(x) g(y), \tag{14}$$

where

$$f(x) = \begin{cases} 1, & 0 < x < \frac{1}{2}\alpha L, \\ \cos^2\left[\dfrac{\pi(x - \frac{1}{2}\alpha L)}{(1-\alpha) L}\right], & \frac{1}{2}\alpha L < x < \frac{1}{2}L, \end{cases}$$

$$g(y) = \begin{cases} 1, & 0 < y < \frac{1}{2}\beta B, \\ \cos^2\left[\dfrac{\pi(y - \frac{1}{2}\beta B)}{(1-\beta) B}\right], & \frac{1}{2}\beta B < y < \frac{1}{2}B. \end{cases}$$

The definition is extended by symmetry to the full rectangle.

5. Solution of the equations

We discuss here the numerical solution of the conservation-of-mass equation (7) and the pair of equations (8), a statement of conservation of momentum. In order to solve these nonlinear time-dependent partial differential equations, we employ a finite-difference method, often referred to as the Modified Euler Method. We note that (7) can be solved explicitly for η_t once u and v are known at a given time, whereas (8) involves time derivatives of u and v as well as of η. The numerical solutions for u and v can be marched in time by means of (8) if we can eliminate the time dependence of η from it. Fortunately this can be done by substituting η_t from (7) into (8). Since it then no longer contains time derivatives of η, (8) can now be solved for u and v.

We shall approximate the continuous variables $\eta(x, y, t)$, $u(x, y, t)$ and $v(x, y, t)$ by the discrete variables $\eta^n_{i,j}$, $u^n_{i,j}$ and $v^n_{i,j}$, where i and j denote mesh points on the x- and y-axes and n denotes a mesh point on the time axis. We denote the space mesh size by $\Delta x\ (= \Delta y)$ and the time mesh size by Δt. We note that in the numerical analysis we have used dimensionless variables with fundamental units ρ, g and h_0. In order to keep track of the variables u and v in the matrix equation that will be obtained from (8) and further to reduce its bandwidth, we introduce a new index m with

$$m = l + 2[(j-1) + (i-1) N_y], \tag{15}$$

where N_y is the number of nodes in the y-direction and $l = 1, 2$ corresponds to u and v respectively. Due to the symmetry of the problem with respect to the x-axis we consider only half of the channel in our computations. To achieve this we regard the x-axis as another wall where the no-flux condition (12) is enforced. Inspection of the momentum equation (8) in the y-direction shows that it is automatically satisfied at the channel walls if $\hat{p}_y = 0$ there.

Because of the necessity of a finite number of mesh points, we also consider two fictitious boundaries far in front of and far behind the disturbance. At these 'open boundaries' we use Sommerfeld's condition with constant phase speed $c = \pm(gh_0)^{\frac{1}{2}}$, mainly because previous work [e.g. Wu & Wu 1982 and Ertekin *et al.* 1984] showed that it is successful in avoiding significant reflection in the problem that we are considering here. This condition may be stated as follows:

$$\Omega_t + c\Omega_x = 0, \tag{16}$$

where Ω may be u, v or η. The above condition, in its rather simplistic form (c being here a constant), has consistently suppressed reflections from the downstream open boundary even though the downstream waves were three-dimensional, criss-crossing the channel.

Having determined the numerical boundary conditions, we approximate in (7) and (8) the spatial derivatives of u, v and η by well-known central-difference formulas and apply to these equations a two-step Modified Euler Method for all the interior nodes of the computational region. Equation (8) results in a finite-difference equation with banded coefficient matrix that must be solved. We note that in the case of the two-dimensional G–N or Boussinesq-type equations the coefficient matrix is a tridiagonal one (Ertekin 1984) and consequently can be solved exactly by the Thomas algorithm (see, e.g. Ames, Lee & Zaiser 1968). Due to the nature of the equations in the three-dimensional case the coefficient matrix that results is a broadbanded matrix. We solve the simultaneous linear equations, therefore, by the successive-over-relaxation method.

To monitor the convergence of the iterated solutions u and v between time steps n and $n+1$, we used a convergence test with a prescribed tolerance γ given by

n+1, k-1

$$\gamma^2 = \sum_{m=1}^{N_T} [f_m^{(n+1,k)} - f_m^{(n+1,k-1)}]^2 \Big/ \sum_{m=1}^{N_T} [f_m^{(n)}]^2, \tag{17}$$

where f is u or v, k is the iteration number, and N_T is the total number of mesh points in the computational domain. The tolerance used, $\gamma = 10^{-4}$, caused k_{max} to vary between 10 and 15 at each time step of the Euler Method (we recall that the Modified Euler Method can be applied in two steps). The maximum iteration number was reduced by optimizing the successive-over-relaxation parameter at the beginning of the computer program. In our calculations the parameter that minimized the number of iterations lay between 1.4 and 1.5.

We note that (7) and (8), which we are solving numerically, are given in a coordinate system fixed in space. Since the pressure is moving in this fixed system, the 'step-shifting-region' technique devised by Wu & Wu (1982) is applied. Even though we have not attempted to solve the G–N equations in a moving frame, one would not expect results different from the fixed-frame case since the G–N equations are Galilean invariant. Nevertheless, we conjecture that the elimination of nodes at the downstream open boundary after each K time steps may help the 'imperfect' open-boundary condition to contaminate less the interior values.

The numerical stability of the two-step scheme used here was discussed by Yeung

(1982) and Ertekin (1984). The stability of the integration scheme can be characterized by an index, ξ. When this index is less than one, the computation is stable, and when it is greater than one, it is unstable. This index for linear equations is

$$\xi^2 = 1 + \tfrac{1}{4}(\Delta t\, k c)^4, \tag{18}$$

where k is the wavenumber. It was found by Ertekin (1984) that the marginal instability indicated by (18) for all choices of Δt had not created any features of an unstable scheme in the solution of the two-dimensional equations. This is mainly because wavelengths are long and cross-waves are not present. In our present three-dimensional computations the downstream waves display their usual complicated structure behind the disturbance and hence the existence of waves with wavenumber $k = \pi/\Delta y$ is inevitable. In fact, these waves with $2\Delta y$ wavelength caused instability in the downstream region, at long times, in the form of wave build-up at the channel walls. In order to remove these numerical waves from the solution we applied a filtering scheme first introduced by Shapiro (1975) and derived independently by Longuet-Higgins & Cokelet (1976). The following five-point formula is used to smooth u and v in the y-direction every five time steps:

$$\bar{f}_{i,j} = \tfrac{1}{16}[-f_{i,j-2} + 4f_{i,j-1} + 10f_{i,j} + 4f_{i,j+1} - f_{i,j+2}], \tag{19}$$

where f is u or v. It was found unnecessary to smooth η since η is explicitly determined by u and v through (7). Our studies have showed that the solitons (their amplitudes and speeds) have not been affected by this filtering.

We have also computed the wave resistance experienced by the pressure distribution. The non-dimensional wave-resistance coefficient is given by

$$C_{\mathrm{wr}} = -\iint \hat{p}\bar{\eta}_{\bar{x}}\, \mathrm{d}\bar{x}\, \mathrm{d}\bar{y}, \tag{20}$$

where bars indicate that variables are dimensionless.

A two-dimensional pressure distribution was used in the present computer program to check the accuracy of the iterated solutions by comparing them with the ones obtained in Ertekin *et al.* (1984). We have found that the iterated solutions for the amplitude and speed of the waves, as well as the wave resistance, differ by less than 10^{-4} from the 'exact' solutions obtained by the Thomas algorithm used in the earlier work. The cross-channel soliton-amplitude drift, typically $\pm 0.4\,\%$, was totally eliminated by the application of filtering. There was no soliton speed variation within the mesh-size limitation of its determinability either before or after filtering. It has also been observed that soliton amplitude varied by $\pm 3\,\%$ (after it has completely separated from the disturbance) along the channel.

All computations presented here were performed on the CDC 7600 of the Lawrence Berkeley Laboratory of the University of California at Berkeley using single precision. The computer program required about 4000 s of execution time for 700 time steps.

6. Results

Computations were made for $\mathbb{F} = 0.9$, 1.0, 1.1, and 1.2 for the following values of the various parameters:

$$\frac{2b}{h_0} = 8, \quad \frac{B}{2b} = \frac{1}{2}, \quad \frac{L}{B} = 2, \quad \overline{P} = \frac{\hat{p}_{\max}}{\rho g h_0} = 0.3, \quad \alpha = 0.7, \quad \beta = 0.4. \tag{21}$$

In addition, for $\mathbb{F} = 1.2$ computations were made for $\overline{P} = 0.1$. Also, $\Delta x/h_0 = 0.2$.

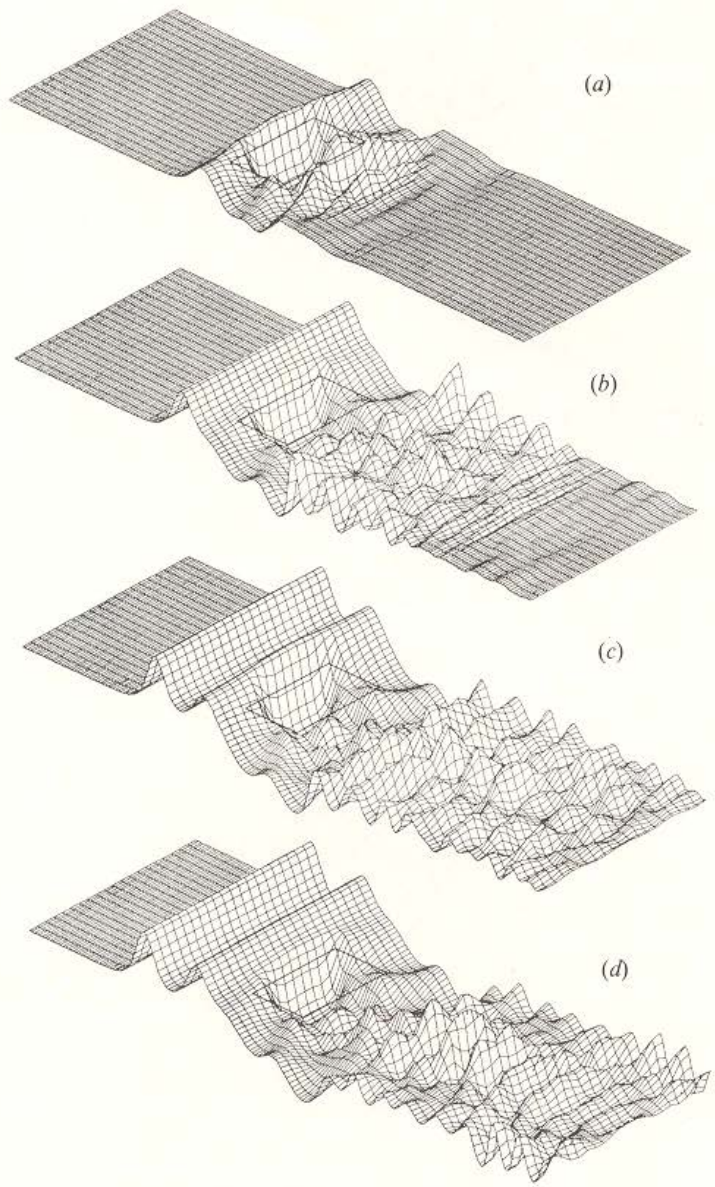

FIGURE 1. Free surface for $\mathbb{F} = 1.0$ and (*a*) $UT/h_0 = 10$, (*b*) 30, (*c*) 50, and (*d*) 60.

From the numerical results contour plots as well as perspective representations for the free surface were prepared for each value of $\mathbb{F}$. For $\mathbb{F} = 0.9$, these were made at intervals $UT/h_0 = 5$, where T is time; for $\mathbb{F} = 1.1$ the interval was 11 and for $\mathbb{F} = 1.0$ and 1.2 it was 10. Although the development of the wave pattern is different in the four cases with $\overline{P} = 0.3$, the most important aspects will be adequately displayed if we show the plots for $\mathbb{F} = 1.0$ up through the appearance of the second soliton and then the last plots for 0.9, 1.0, 1.1. (We defer the two cases where $\mathbb{F} = 1.2$ until later.) These are shown in figures 1 and 2. It is evident that, in all cases, solitons are being generated that escape from the moving pressure distribution and move ahead of it. The surfaces following the pressure distribution are complicated doubly corrugated ones, much different in character from the waves in front of the disturbance. One should note that in figures 1, 2, 5, 6, 7 and 8 the horizontal scale is exaggerated and that the displayed length of the free surface is actually 10 times its width although it appears to be only 3 times.

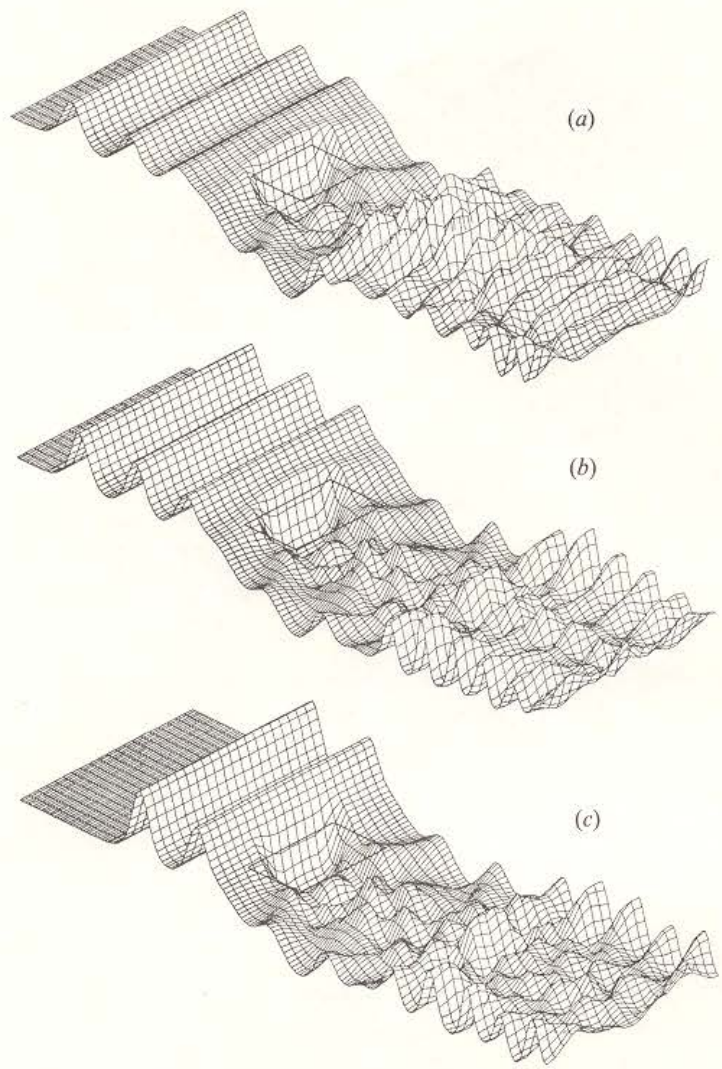

FIGURE 2. Free surface for (a) $\mathbb{F} = 0.9$, $UT/h_0 = 70$, (b) $\mathbb{F} = 1.0$, $UT/h_0 = 90$, and (c) $\mathbb{F} = 1.1$, $UT/h_0 = 77$.

Qualitatively the behaviour conforms to that observed with ship models in a towing tank, with one exception. In the experiments the solitons would begin to break as $\mathbb{F}$ approached 1.2 and would barely be able to escape from the model. For $\mathbb{F} > 1.2$, instead of a soliton a hydraulic jump would be formed, also spanning the tank like the solitons, and would accompany the model down the tank. If discontinuous solutions (hydraulic jumps) are to be admitted as solutions, then the G–N equations must be supplemented by jump conditions, as is customary in the theory of hydraulic jumps or of shock waves. Such conditions have been discussed by Green & Naghdi (1976*a*), but we do not attempt to deal with this problem here.

Our experience with computations was different. For a particular value of $\overline{P}$ there appears to be a limiting value of $\mathbb{F}$ beyond which no solitons escape. In this region of high Froude numbers the free-surface disturbance is eventually local, for the initial starting disturbance is gradually left behind. This behaviour is also apparent in results of the two-dimensional form of the G–N equations (Ertekin *et al.* 1984). Computations were performed for $\mathbb{F} = 1.2$, for a moving two-dimensional pressure distribution

$$\hat{p} = \frac{\rho g h_0 \overline{P} \cos^2 \pi x}{L}, \quad |x| < \tfrac{1}{2}L,$$

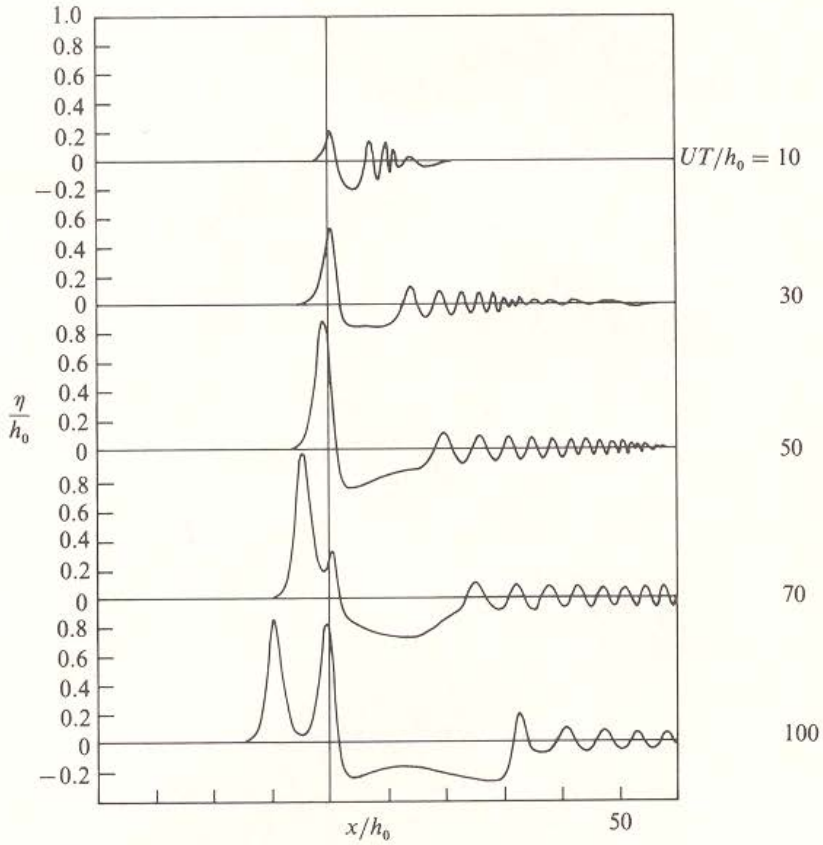

FIGURE 3. Free surface generated by a moving two-dimensional pressure band with $\mathbb{F} = 1.2$, $\overline{P} = 0.3$.

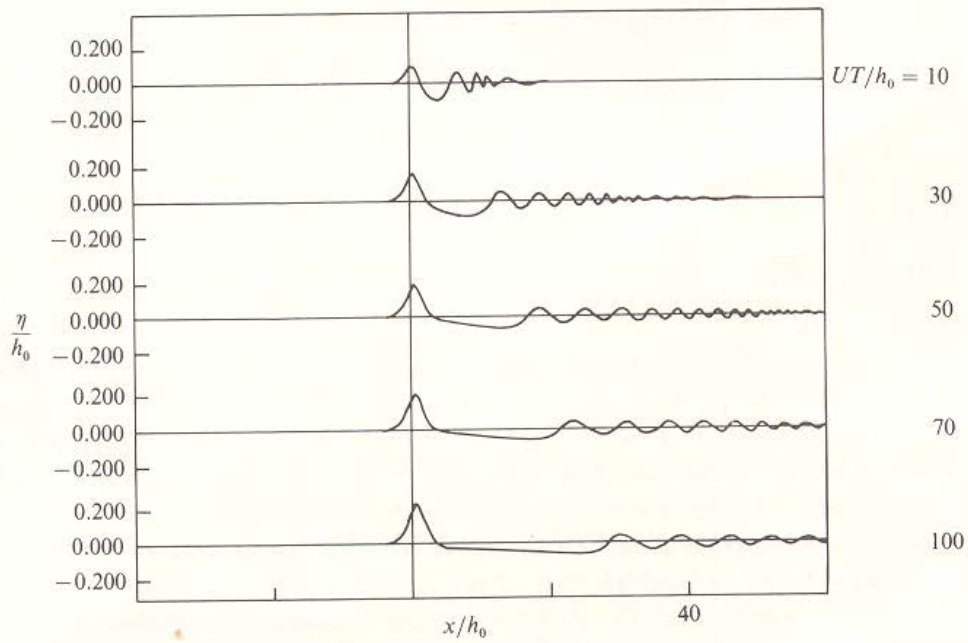

FIGURE 4. Free surface generated by a moving two-dimensional pressure band with $\mathbb{F} = 1.2$, $\overline{P} = 0.15$.

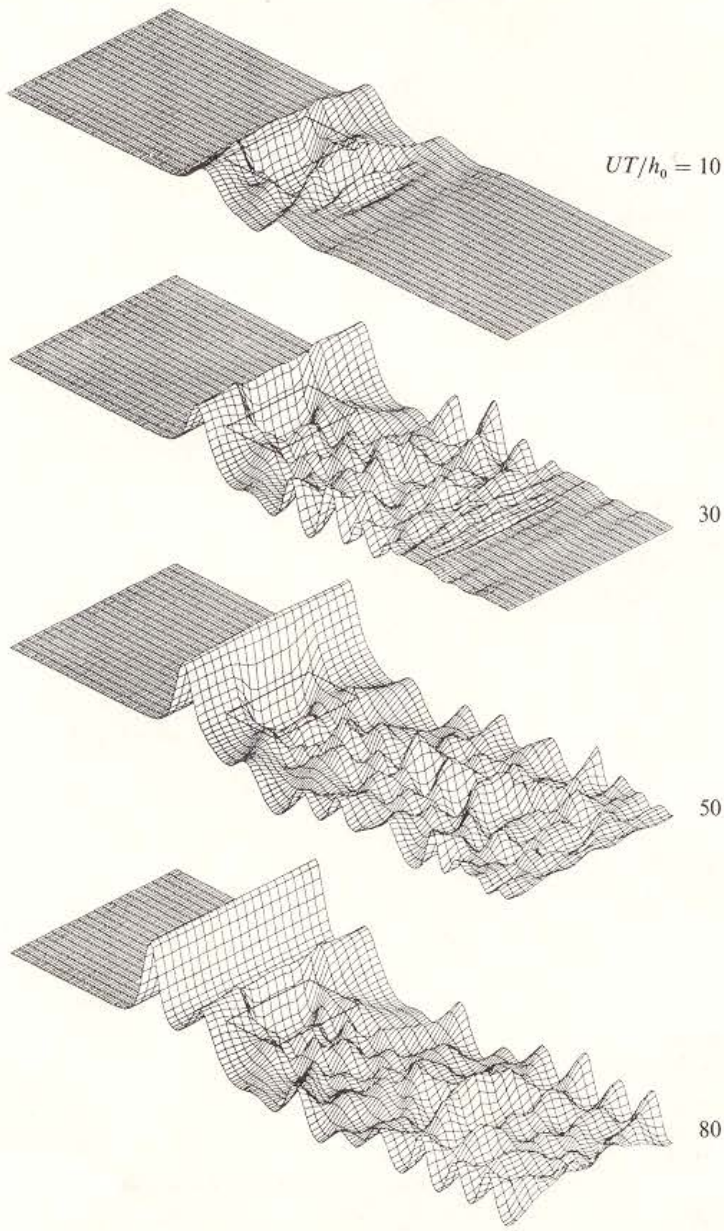

FIGURE 5. Free surface for $\mathbb{F} = 1.2$, $\overline{P} = 0.30$ and $UT/h_0 = 10$, 30, 50, and 80.

and for two values of $\overline{P}$. Figure 3 shows the results for $\overline{P} = 0.3$ and figure 4 for $\overline{P} = 0.15$. These figures display the free-surface profiles η/h_0 at successive values of UT/h_0 at intervals of 20 and show rather strikingly the two types of behaviour. For 0.15 no solitons are produced, the disturbance is left behind and a lengthening depression whose depth decreases with time follows the pressure distribution. For 0.3, solitons are escaping and a lengthening depression of approximately constant depth follows the pressure distribution.

Figures 5 and 6 show analogous behaviour for the three-dimensional rectangular pressure distributions. Both are for $\mathbb{F} = 1.2$ and show perspective views of η/h_0 for $UT/h_0 = 10$, 30, 50 and 80; figure 5 is for $\overline{P} = 0.3$, figure 6 for 0.1. Figure 5 is qualitatively similar to those already shown for lower values of $\mathbb{F}$: solitons are formed

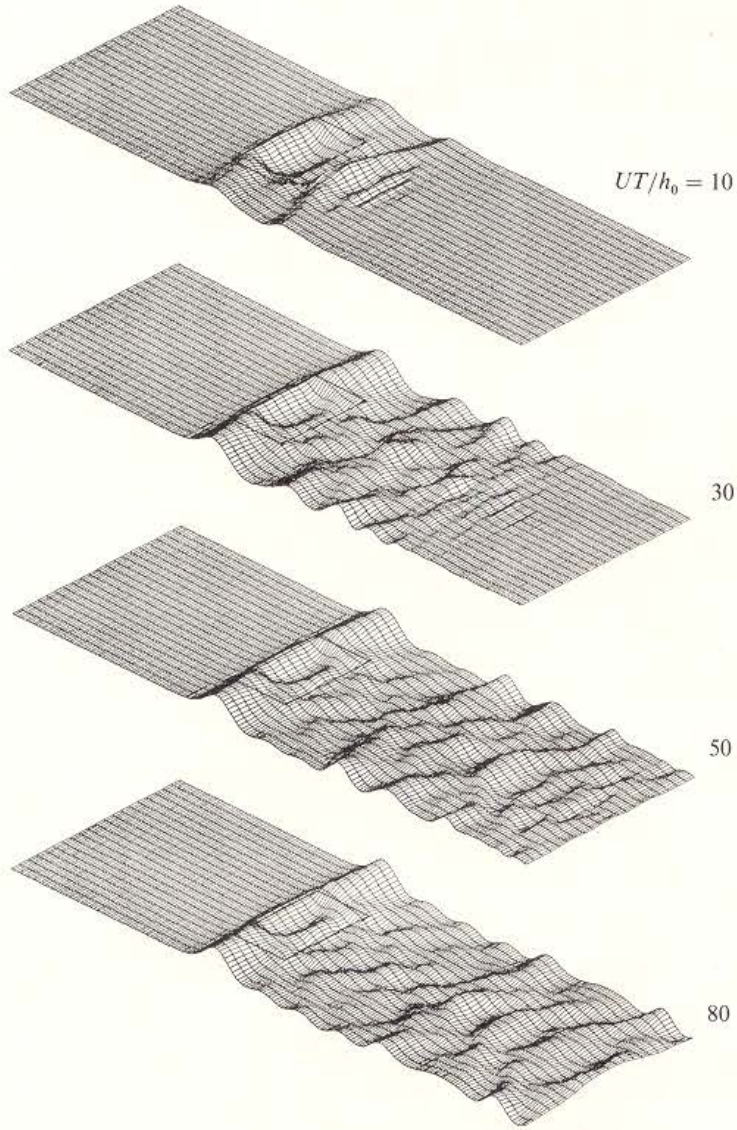

FIGURE 6. Free surface for $\mathbb{F} = 1.2$, $\overline{P} = 0.10$ and $UT/h_0 = 10$, 30, 50, and 80.

and a substantial doubly corrugated disturbance follows the pressure distribution. In figure 6, on the other hand, no solitons are formed. In the immediate neighbourhood of the pressure distribution a nearly invariant wave pattern develops, one that spans the tank but is not really two-dimensional. Further behind, a gradually lengthening slight depression appears. That this really is a depression shows up much more clearly in the contour plots. Figures 7 and 8 show these for $\overline{P} = 0.3$ and 0.1 respectively, for $UT/h_0 = 80$. As one can see, the pressure distribution is followed by a (lengthening) depression for $\overline{P} = 0.3$, as in the two-dimensional computations. However, the depth of the depression does not appear to be decreasing with time as it does for 0.1.

The different behaviour for the two values of $\overline{P}$ is also reflected in the wave resistance. Figure 9 shows the wave-resistance coefficient C_{wr} computed for the three-dimensional pressure distribution as a function of UT/h_0 for $\mathbb{F} = 1.0$, 1.1, 1.2 and $\overline{P} = 0.3$, and for $\mathbb{F} = 1.2$, $\overline{P} = 0.1$. The first three cases are typical of C_{wr} when solitons are being generated. After an initial transient there is an oscillation about a constant value with a period equal to that of soliton generation. For the last case,

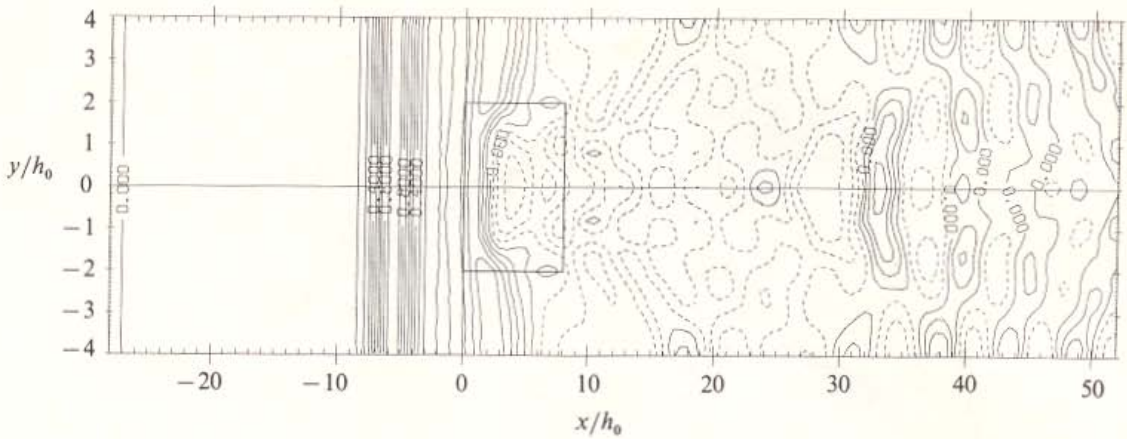

FIGURE 7. Contour map of free surface for $\mathbb{F} = 1.2$, $\overline{P} = 0.30$, and $UT/h_0 = 80$.

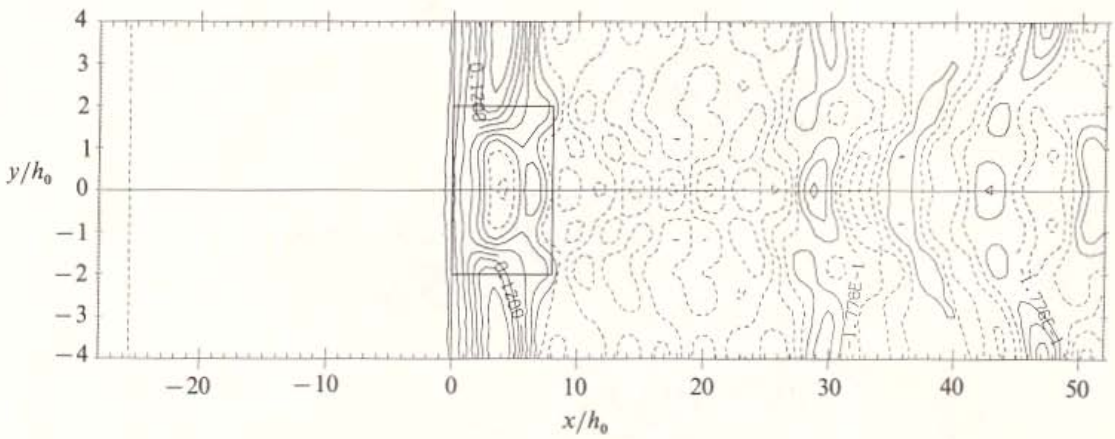

FIGURE 8. Contour map of free surface for $\mathbb{F} = 1.2$, $\overline{P} = 0.10$, and $UT/h_0 = 80$.

however, where no solitons are being generated, there is a steady decrease in C_{wr} following the initial transient. We assume, in conformity with the two-dimensional behaviour, that C_{wr} approaches zero. Indeed, it is already very small for $UT/h_0 > 50$.

For each value of $\overline{P}$ there appears to be a critical Froude number $\mathbb{F}_{\mathrm{crit}}$ beyond which no solitons are generated and the wave resistance decreases to zero as UT/h_0 increases. To determine this function numerically would be prohibitively expensive in three dimensions, but inexpensive to do in two. The two-dimensional C_{wr} was computed as a function of $\mathbb{F}$ for $\overline{P} = 0.10, 0.15, 0.20, 0.25, 0.30$ and 0.40. When $\overline{P} = 1$, the static free-surface depression (i.e. the fictitious ship) touches the bottom. Thus, values of $\overline{P}$ approaching 1 may not be appropriate. Figure 10 shows $\overline{C}_{\mathrm{wr}} = C_{\mathrm{wr}}/\overline{P}^2$ plotted against $\mathbb{F}$. If $\mathbb{F}$ is low enough all of the curves appear to collapse near the line $\overline{C}_{\mathrm{wr}} = 2.85(1-\frac{1}{2}\mathbb{F})$. As $\mathbb{F}$ increases $\overline{C}_{\mathrm{wr}}$ first increases above this line and then drops rapidly to zero. From figure 10 one finds $\mathbb{F}_{\mathrm{crit}} \approx 1+\overline{P}/(0.7+\overline{P})$. This function is shown in figure 11.

These results are remarkable in several ways. It is surprising that the resistance associated with the essentially nonlinear process of soliton generation is proportional to $\overline{P}^2$, a result usually associated with linear theories. Figure 10 appears to imply that no periodic soliton generation will occur for $\mathbb{F} > 2$. However, we have not verified this result. Figure 11 indicates that steady solutions for the given sinusoidal shape of pressure distribution occur only for combinations of $\mathbb{F}$ and $\overline{P}$ that lie above the

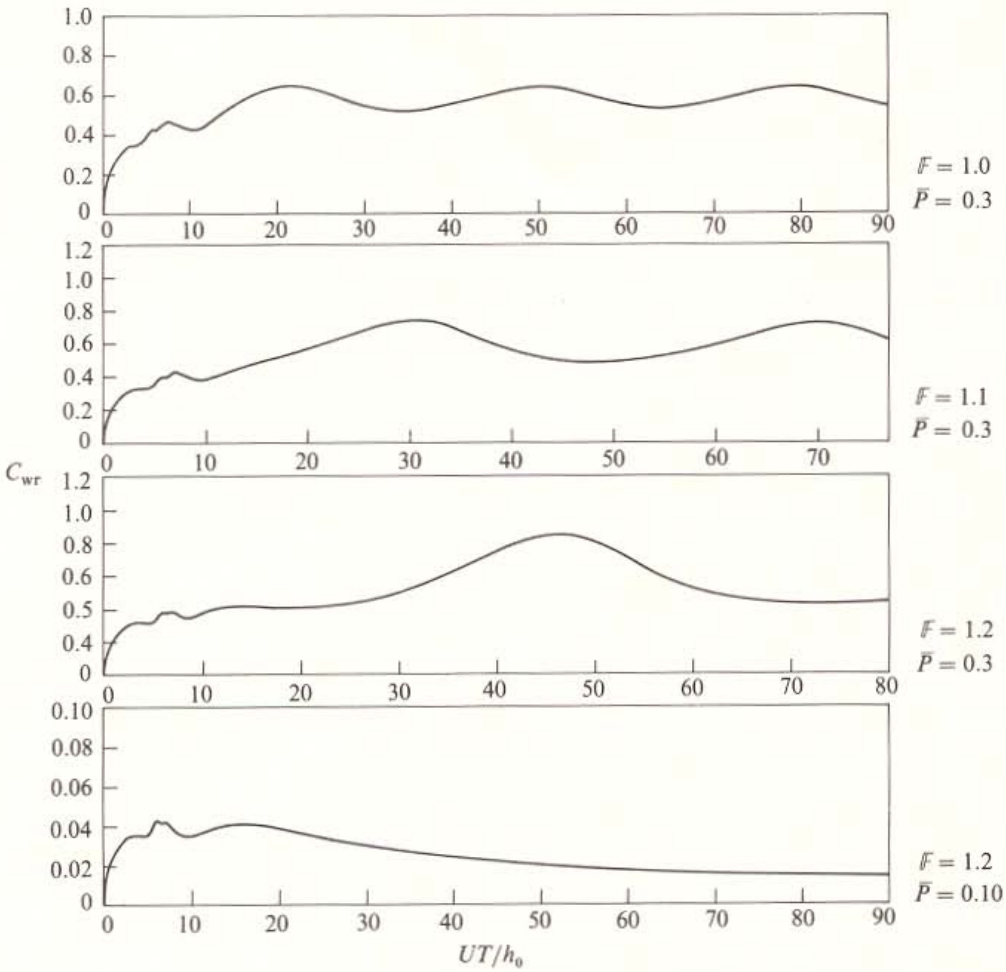

FIGURE 9. Wave resistance coefficient as a function of UT/h_0 for $\mathbb{F} = 1.0$, 1.1, 1.2 and $\bar{P} = 0.30$, and $\mathbb{F} = 1.2$ and $\bar{P} = 0.10$.

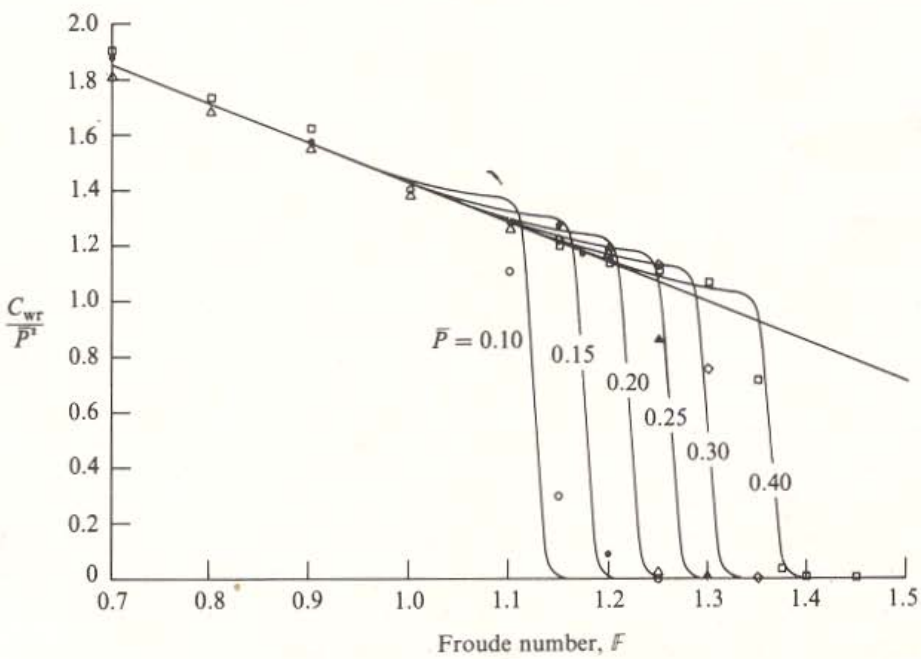

FIGURE 10. $C_{wr}/\bar{P}^2$ as a function of $\mathbb{F}$.

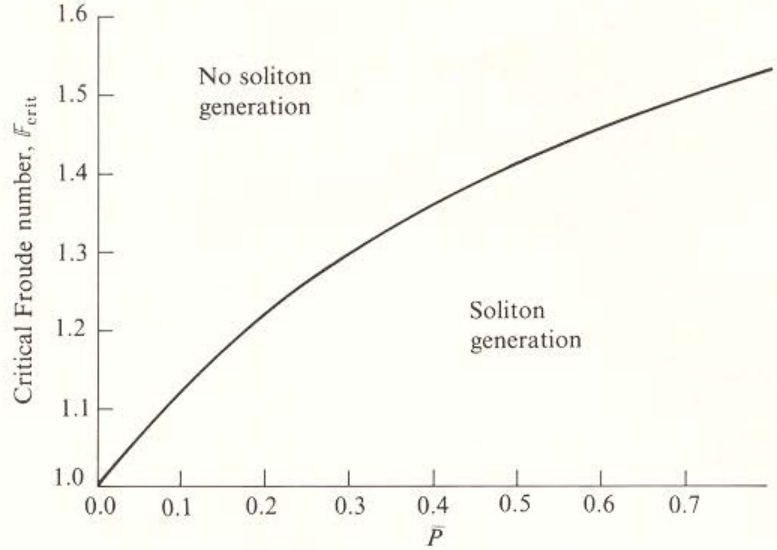

FIGURE 11. $\mathbb{F}_{crit}$ as a function of $\bar{P}$.

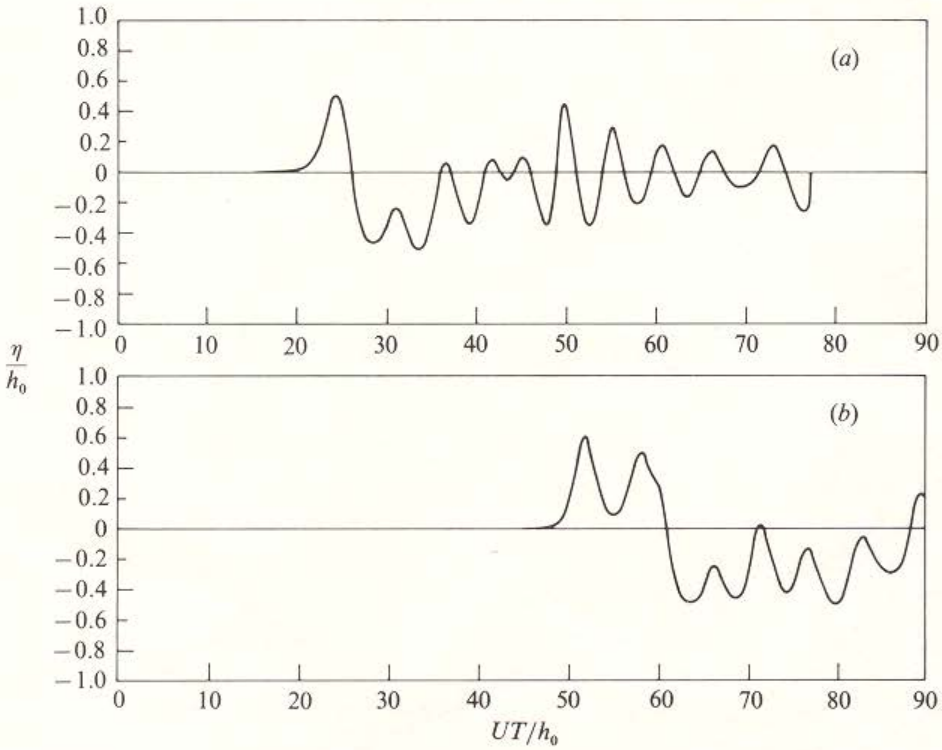

FIGURE 12. Calculated wave records at points (a) $25h_0$ and (b) $60h_0$ ahead of the initial point of pressure distribution; $\mathbb{F} = 1.0$.

curve. We anticipate that other shapes of pressure distribution would exhibit a similar behaviour.

In addition to the perspective and contour plots, we have also computed wave profiles as they would have been perceived by gauges fixed in the tank at distances $25h_0$ and $60h_0$ ahead of the initial position of the pressure distribution. These are shown for $\mathbb{F} = 1.0$ in figure 12. For comparison, experimentally determined curves are shown in figure 13. In this case the gauges were placed approximately $65h_0$ and $130h_0$ ahead of the model in its starting position. Both the calculated and measured

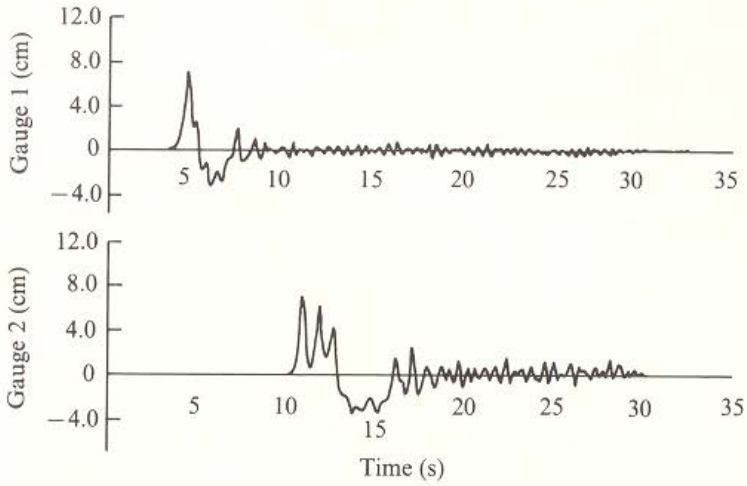

FIGURE 13. Measured wave records taken at gauges fixed in the towing tank approximately $65h_0$ and $130h_0$ ahead of initial position of model; $\mathbb{F} = 1.0$.

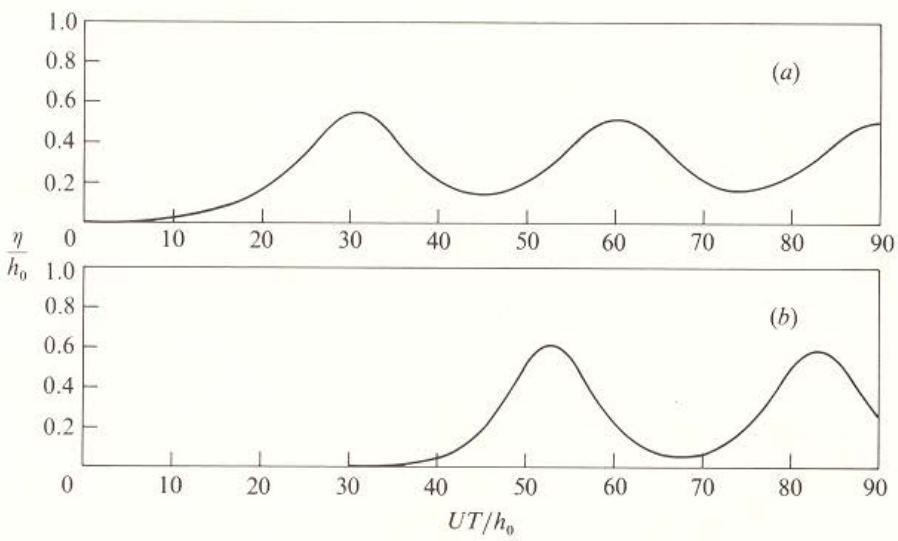

FIGURE 14. Calculated wave records at points (*a*) $2h_0$ and (*b*) $8h_0$ ahead of the moving pressure distribution; $\mathbb{F} = 1.0$.

curves show waviness in the depression following the pressure distribution or model, something not present in the two-dimensional case (see figure 3).

We have also computed the waves that would have been recorded by moving gauges situated $2h_0$ and $8h_0$ ahead of the pressure distribution. These are shown in figure 14 for $\mathbb{F} = 1.0$. For comparison we show again for $\mathbb{F} = 1.0$ some measured records from moving gauges situated $3h_0$ and $5h_0$ ahead of the model. The qualitative similarity is evident. Figure 15 includes also the measured resistance coefficient. Although this includes frictional and form resistance as well as wave resistance, the similarity to the top C_{wr} curve in figure 9 is evident. Even the little jog just before the oscillation is present, as it is on other measured resistance curves.

From the numerical printouts of the solutions it is possible to determine with reasonable accuracy the soliton amplitude and speed and also the frequency of generation. Since the amplitude increases during the initial instants, it was taken at the last calculated value of UT/h_0. The speed relative to the pressure distribution

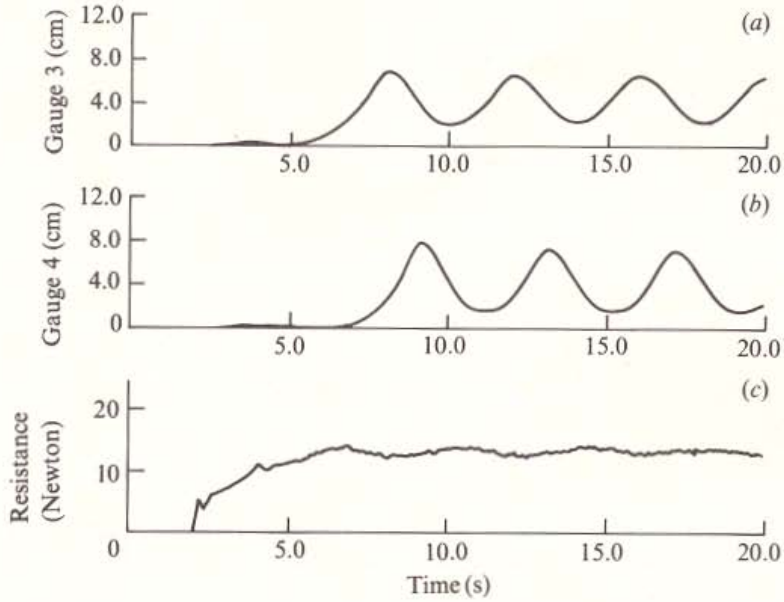

FIGURE 15. Measured wave records from gauges attached to the towing carriage (*a*) $3h_0$ and (*b*) $5h_0$ ahead of the model; $\mathbb{F} = 1.0$. (*c*) The measured wave resistance of the model.

$\mathbb{F}$	A/h_0	$c/(gh_0)^{\frac{1}{2}}$	$(1+A/h_0)^{\frac{1}{2}}$
0.9	0.5101	1.224	1.229
1.0	0.6248	1.280	1.275
1.1	0.7729	1.340	1.332
1.2	0.9577	1.390	1.399

TABLE 1. Amplitudes and speeds of first solitons

$\mathbb{F}$	0.9	1.0	1.1
UT_g/h_0	20.0	29.6	39.3

TABLE 2. Dimensionless period of generation of solitons

was determined from the last two values of UT/h_0 and then converted to absolute speed. The results for the leading soliton are shown in table 1.

The last column of table 1 also shows the steady-state speed associated with amplitude according to

$$\frac{c^2}{gh_0} = 1 + \frac{A}{h_0}, \tag{22}$$

a formula given originally by Rayleigh (1876), but appearing also in the Green–Naghdi (Green, Laws & Naghdi 1974) theory. There is some inaccuracy in the determination of $c/(gh_0)^{\frac{1}{2}}$ because mesh size limits the accuracy with which the position of a peak can be determined. However, the values conform well with the theoretical values for an isolated soliton.

The period of soliton generation T_g is determined from the time interval between the peaks of the first and second solitons at the first numerical moving wave gauge

S	$\mathbb{F} = 0.9$	1.0	1.1
0.1134	30	35	38
0.0946	33	38	43
0.0941	35	42	47

TABLE 3. Some measured values of UT_g/h_0

located $2h_0$ ahead of the pressure distribution. The results are shown in table 2. The value of T_g for $\mathbb{F} = 1.2$ could not be determined, for the peak of the second soliton had not appeared before the last value of UT/h_0 for which calculations were made.

No precise comparison can be made with experimental values, for the experiments were made with a ship model and the calculations with a pressure distribution. Nevertheless, a crude comparison is possible. One conclusion from the experiments was that the dimensionless period UT_g/h_0 was chiefly determined by the blockage coefficient, S = midship section area/$2bh_0$. By using the hydrostatically displaced free surface $\hat{p}/\rho g$ as a crude equivalent of a ship, one finds from (14) that

$$S_{\mathrm{pd}} = \frac{B}{4b}(1+\beta)\,\overline{P} = 0.105$$

with the values from (21). In Ertekin (1984) one can find data for three values of S: 0.113 ($2b/h_0 = 9.76$), 0.0946 ($2b/h_0 = 8.13$), and 0.0941 ($2b/h_0 = 12.2$). The corresponding measured values of UT_g/h_0 are shown in table 3. The agreement is not impressive, and was not expected to be, but is mostly within 50 % of the computed values. Both calculated and measured values show the same rising trend as $\mathbb{F}$ increases.

7. Concluding remarks

It seems clear from the preceding section that the G–N equations are able to predict behaviour for a moving pressure distribution very similar to that observed for a moving ship model in a towing tank. However, we do not think that this is a property unique to the G–N equations. In particular, Wu's equations would almost certainly yield qualitatively similar results. This suggests a mathematical problem, that of determining the class of equations that generate solitons ahead of a three-dimensional disturbance moving along a canal, while still producing a complex wave pattern behind it.

This research has been sponsored by the Office of Naval Research under Contract N000014-84-K-0026.

REFERENCES

AKYLAS, T. R. 1984 On the excitation of long nonlinear water waves by a moving pressure distribution. *J. Fluid Mech.* **141**, 455–466.

AMES, W. F., LEE, S. Y. & ZAISER, J. N. 1968 Nonlinear vibration of a traveling threadline. *Intl J. Non-linear Mech.* **3**, 449–469.

COLE, S. L. 1985 Transient waves produced by flow past a bump. *Wave Motion* **7**, 579–587.

ERTEKIN, R. C. 1984 Soliton generation by moving disturbances in shallow water: theory, computation and experiment. Ph.D. dissertation, University of California, Berkeley.

Ertekin, R. C., Webster, W. C. & Wehausen, J. V. 1984 Ship-generated solitons. *Proc. 15th Symp. Naval Hydrodynam., Hamburg*, pp. 347–364.

Graff, W. 1962 Untersuchungen über die Ausbildung des Wellenwiderstandes im Bereich der Stauwellengeschwindigkeit in flachem, seitlich beschränktem Fahrwasser. *Schiffstechnik* **9**, 110–122.

Green, A. E., Laws, N. & Naghdi, P. M. 1974 On the theory of water waves. *Proc. R. Soc. Lond.* A**338**, 43–55.

Green, A. E. & Naghdi, P. M. 1976*a* Directed fluid sheets. *Proc. R. Soc. Lond.* A**347**, 447–473.

Green, A. E. & Naghdi, P. M. 1976*b* A derivation of equations for wave propagation in water of variable depth. *J. Fluid Mech.* **78**, 237–246.

Green, A. E. & Naghdi, P. M. 1977 Water waves in a nonhomogeneous incompressible fluid. *Trans. ASME* E: *J. Appl. Mech.* **44**, 523–528.

Huang, De-Bo, Sibul, O. J. & Wehausen, J. V. 1982*a* Ships in very shallow water. *Festkolloquium zur Emeritierung von Karl Wieghardt, März 1982*, Institut für Schiffbau der Universität Hamburg, Bericht Nr. 427 (April 1983), pp. 29–49.

Huang, De-Bo, Sibul, O. J., Webster, W. C., Wehausen, J. V., Wu, De-Ming & Wu, T. Y. 1982*b* Ships moving in the transcritical range. *Conf. on Behaviour of Ships in Restricted Waters, Varna. Proc.* vol. 2, pp. 26/1–26/10.

Longuet-Higgins, M. S. & Cokelet, E. D. 1976 The deformation of steep surface waves on water. I. A numerical method of computation. *Proc. R. Soc. Lond.* A**350**, 1–26.

Mei, C. C. 1986 Radiation of solitons by slender bodies advancing in a shallow channel. *J. Fluid Mech.* **162**, 53–67.

Rayleigh, Lord 1876 On waves. *Phil. Mag.* (5) **1**, 257–279. (*Scientific papers* **1**, 251–271.)

Shapiro, R. 1975 Linear filtering. *Maths Comput.* **29**, 1094–1097.

Sturtzel, W. & Graff, W. 1958 Untersuchungen der in stehendem und strömendem Wasser festgestellten Änderungen des Schiffswiderstandes durch Druckmessungen. *Forschungsberichte des Wirtschafts- und Verkehrsministeriums Nordrhein-Westfalen, Nr.* 618, 34 pp.

Thews, J. G. & Landweber, L. 1935 The influence of shallow water on the resistance of a cruiser model. *U.S. Experimental Model Basin, Navy Yard, Washington, D.C., Rep. No.* 408, 31 pp.

Wu, T. Y. 1981 Long waves in ocean and coastal waters. *J. Engng Mech. Div. ASCE* **107**, 501–522.

Wu, De-Ming & Wu, T. Y. 1982 Three-dimensional nonlinear long waves due to moving surface pressure. *Proc. 14th Symp. Naval Hydrodynam., Ann Arbor, Mich.*, pp. 103–129.

Yeung, R. W. 1982 Numerical methods in free-surface flows. *Ann. Rev. Fluid Mech.* **14**, 395–442.